


# Omnidirectional Conformal Cloak Without Geometrical Dispersion

Yichao Liu,<sup>1</sup> Fei Sun,<sup>1,†</sup> and Sailing He<sup>2,3,\*</sup>

<sup>1</sup>Key Lab of Advanced Transducers and Intelligent Control System, Ministry of Education and Shanxi Province, College of Physics and Optoelectronics, Taiyuan University of Technology, Taiyuan, 030024, China

<sup>2</sup>State Key Laboratory of Modern Optical Instrumentations, Centre for Optical and Electromagnetic Research, JORCEP, East Building #5, Zijingang Campus, Zhejiang University, Hangzhou 310058, China

<sup>3</sup>Department of Electromagnetic Engineering, School of Electrical Engineering, Royal Institute of Technology (KTH), S-100 44 Stockholm, Sweden

 (Received 7 March 2018; revised manuscript received 24 October 2019; published 4 December 2019)

The phase delay problem of invisibility cloaks designed by optical conformal mapping is referred to the optical path difference between the waves in upper and lower Riemann sheets. As the frequency changes, the phase delay varies accordingly (here, we call it geometrical dispersion), which restricts the cloaks to working only at some discrete frequencies. Here, we solve the phase-delay problem by placing an optically null medium in the lower Riemann sheet. The conformal cloaks designed by using our method have many advantages, such as a continuous working band (no geometrical dispersion), omnidirectionality, robustness under frequency shifts, and no need for any complex materials that are both anisotropic and inhomogeneous. We also design metallic microchannels to realize our cloaks.

DOI: [10.1103/PhysRevApplied.12.064009](https://doi.org/10.1103/PhysRevApplied.12.064009)

## I. INTRODUCTION

Transformation optics (TO) [1–6] has aroused interest in invisibility cloaks [7–11] over the last decade. Two different methods are proposed in initial examples to give cloaks of different index profiles [4,5]. The first method proposed by Pendry *et al.* [4], usually referred to as TO, is based on Maxwell's equations and is theoretically perfect for waves (as verified by experimental demonstrations [12]). However, the complex material requirements (inhomogeneous anisotropic materials with singularities at the inner boundary) restrict their real applications. The second method proposed by Leonhardt [5], usually referred to as optical conformal mapping (OCM), is based on Fermat's principle and the Helmholtz equation. Therefore, it is theoretically only valid within the realm of geometry optics [5]. When used for waves, there are several problems, one of which is the phase-delay problem [13] and another is the large index range in the interior of the branch cut. As a consequence, no experimental demonstrations of omnidirectional OCM cloaks have been made. Up until now, only one experimental demonstration of truncated unidirectional OCM cloaks has been given by our group [14]. Here, considering the imperfections of the OCM theory for waves, we place an optically null medium in the lower Riemann sheet to solve the phase-delay problem and achieve omnidirectional OCM cloaks that function well for both

rays and waves within some frequency band. At the same time, we change the refractive index in the interior of the branch cut from the previous large distribution range to a homogenous optically null medium (ONM) [15,16], which may simplify the implementation and is more robust under frequency shifts.

We first recall the concept of the Zhukovski transformation (an OCM to design invisibility cloaks [5]), and describe the phase-delay problem [6]. The Zhukovski transformation is one type of conformal mapping given by

$$w = z + \frac{a^2}{z} \quad \text{or} \quad z = \frac{1}{2} \left( w \pm \sqrt{w^2 - 4a^2} \right), \quad (1)$$

where  $z = x + iy$  and  $w = u + iv$  denote complex coordinates in the physical space and the reference space, respectively;  $a$  represents the size of the branch cut in the reference space (line segment with length  $4a$ ) and in the real space (circle with radius  $a$ ). In the language of TO, it maps the lower and upper Riemann sheets in the reference space to the interior and exterior of the circular branch cut in the physical space, respectively. The Zhukovski transformation could only have a cloaking effect with the help of an effective optical design in the lower Riemann sheet, which would guide the ray back to the upper Riemann sheet without producing any reflections or changing the direction of propagation [5]. Many optical instruments may fulfill this requirement, such as a Maxwell fish-eye lens [17–20], an Eaton lens [21–23], or well-arranged mirrors [24]. Although all of these optical instruments can guide the rays

\*sailing@kth.se

†sunfei@zju.edu.cn

(which have touched the branch cut) back to the upper Riemann sheet, they inevitably introduce an additional optical path difference (compared with rays that do not touch the branch cut), i.e., a phase delay. As the wavelength changes, the phase delay varies accordingly, which leads to geometrical dispersion for all previous cloaks designed by conformal mapping under the configuration of double Riemann sheets. Unlike material dispersion (due to the nature of metamaterials), the geometrical dispersion is due to the geometry corresponding to conformal mappings with double Riemann sheets, which leads to discrete working-frequency features [21,25,26]. The geometrical dispersion and materials' dispersion together would restrict the bandwidth of optical conformal cloaks. The purpose of this study is to eliminate the geometrical dispersion. In our previous work, negative index materials are used to eliminate the geometrical dispersion [21]. However, numerical simulations of OCM cloaks with negative index materials are not good as theoretically expected [21].

Here, we use an ONM designed by optical surface transformation to replace the conventional optical instruments and fix the phase-delay problem. In an ONM, the refractive index approaches zero along its principal axis ( $n_{\parallel} = 0$ ) and is infinitely large in directions perpendicular to the principal axis ( $n_{\perp} = 1/n_{\parallel} = \infty$ ). The amplitude and phase of waves at the two ends of an ideal ONM are preserved [16,27,28] because, when waves propagate inside the ONM, the phase delay ( $\Delta\phi$ ) along its principal axis is equal to zero, i.e.,  $\Delta\phi = 2\pi n_{\parallel} \Delta l / \lambda = 0$ , where  $\Delta l$  is the effective length of the ONM along its principal axis and  $\lambda$  is the wavelength of light in a vacuum. In this sense, the ONM performs like a highly directional waveguide that can guide the incident waves or rays (for arbitrary incident angles) along its principal axis direction without producing any phase delay. We can also design an ONM to form a closed loop on the lower Riemann sheet that can redirect the rays to their original direction without producing any phase delay. In practical applications, it is both unnecessary and impossible to make the refractive index on the principal axis strictly equal to zero.

## II. THEORY

Now we move to the design step and show how to use the ONM in the lower Riemann sheet of the Zhukovski transformation to solve the phase-delay problem of OCM cloaks. The basic setup for the cloak is shown in Fig. 1. In the reference space of the Zhukovski transformation, the trajectories of two rays with orthogonal directions are shown in Fig. 1(a). The parallel ray (colored blue) does not touch the branch cut (line segment colored yellow) and propagates in the upper Riemann sheet constantly, while the perpendicular ray (colored red) touches the branch cut and enters the lower Riemann sheet. A donut filled with the ONM is placed in the lower Riemann sheet, the outer

and inner radii of which are  $R_2$  and  $R_1$ , respectively. The principal axis of the ONM is along the tangential direction of the donut, as shown by the blue and white rings in Fig. 1(a). The branch cut is on the radial direction with a size of  $4a = R_2 - R_1$ . The red ray propagates along the principal axis of the ONM for one loop; returns to the upper Riemann sheet, where it falls down; and restores its original direction (no phase delay,  $\Delta\phi = 0$ , and no reflections). Notably, although we only show the normal incident ray, other rays with arbitrary incident angles can also restore their original directions. The reason is that the ONM does not disturb the phase distributions of the waves before they enter the branch cut or after they return (no phase delay) and the wave vector is also unchanged, i.e., the branch cut appears transparent to the waves. In the physical space, as shown in Fig. 1(b), the blue ray bypasses the circular branch cut (yellow circle) and the red ray crosses the circular branch cut. A general coordinate transformation (without extreme stretching or compressing) will not change the values of the permittivity and permeability of the ONM because the permittivity and permeability tensors with components of  $\infty$  (or 0) remain  $\infty$  (or 0) after a transformation. However, the directions of the principal axes of ONMs change after a transformation [27]. For the Zhukovski transformation, the principal axes of the designed ONMs are transformed from concentric circles to the shapes indicated by the blue and white curves in Fig. 1(b), which act as microchannels that connect the upper half and lower half of the branch cut in physical space. The two gray regions in Fig. 1(b) are the cloaking regions, which correspond to the interior of the donut

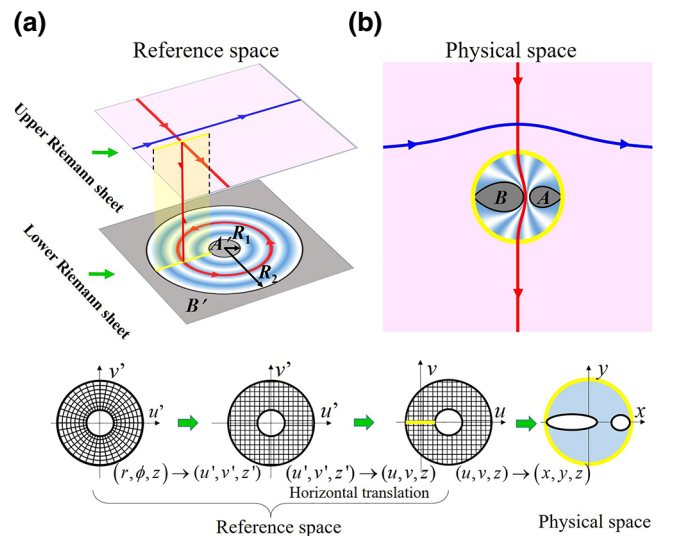


FIG. 1. Design diagram of the cloak. Red and blue lines (curves) are the ray trajectories in (a) the reference space and (b) the physical space. The regions  $A$  and  $B$  colored gray in (b) are cloaking regions corresponding to  $A'$  and  $B'$  in (a), respectively. (c) Design steps of the ONM parameters for the cloak.

( $r < R_1$ ) and the exterior of the donut ( $r > R_2$ ) in Fig. 1(a) (colored gray). We can place any objects inside the gray regions in Fig. 1(b) without disturbing the field distributions outside. The refractive index outside the branch cut in the physical space [regions colored pink in Fig. 1(b)] can be calculated as [5]

$$n = n_w \left| 1 - \frac{a^2}{z^2} \right|, \quad (2)$$

where  $n_w = 1$  is the background index of the reference space. For the interior of the branch cut, the permittivity and permeability can be deduced by the following steps, which are also shown in Fig. 1(c). First, we write the parameter matrix of the ONMs [region of the donut with perfect magnetic conductor (PMC) boundaries] in the cylindrical coordinates ( $r, \varphi, z$ ) of the reference space, shown as the first plot in Fig. 1(c), as follows:

$$\varepsilon'_{(r\varphi)} = \mu'_{(r\varphi)} = \begin{pmatrix} \Delta & 0 & 0 \\ 0 & 1/\Delta & 0 \\ 0 & 0 & \Delta \end{pmatrix}, \quad (3)$$

where  $\Delta$  approaches zero for an ideal ONM. Second, we express the parameters of the ONMs in the reference space in the Cartesian coordinate system ( $u', v', z'$ ), shown as the second plot in Fig. 1(c), as follows:

$$\varepsilon'_{(u'v')} = \mu'_{(u'v')} = M \varepsilon'_{(r\varphi)} G^{-1} M^T, \quad (4)$$

where

$$M = \begin{pmatrix} \partial u'/\partial r & \partial u'/\partial \phi & 0 \\ \partial v'/\partial r & \partial v'/\partial \phi & 0 \\ 0 & 0 & 1 \end{pmatrix} = \begin{pmatrix} \cos(\phi) & -r \sin(\phi) & 0 \\ \sin(\phi) & r \cos(\phi) & 0 \\ 0 & 0 & 1 \end{pmatrix}, \quad (5)$$

and  $G = \text{diag}(1, r^2, 1)$ . Third, we express the ONM in the reference space in a translated Cartesian coordinate system ( $u = u' + (R_2 - R_1)/2$ ,  $v = v'$ ,  $z = z'$ ) to move the donut to a position where the branch cut (from  $-2a$  to  $2a$ ) is located between the inner and outer boundaries of the donut ( $R_2 - R_1 = 4a$ ) [see the third plot in Fig. 1(c)], and the resulting parametric matrix is

$$\varepsilon'_{(uv)} = \mu'_{(uv)} = \varepsilon'_{(u'v')} \left( u - \frac{R_2 - R_1}{2}, v, z \right). \quad (6)$$

Finally, we transform the donut filled with ONMs expressed in Eq. (6) in the reference space to the interior

of the branch cut in the physical space via the Zhukovski transformation [see the last plot in Fig. 1(c)],

$$\varepsilon_{(xy)} = \mu_{(xy)} = \frac{\Lambda \varepsilon'_{(uv)} \Lambda^T}{\det(\Lambda)}, \quad (7)$$

where  $\Lambda$  is the Jacobian matrix representing the Zhukovski transformation in Eq. (1) from the reference space ( $u, v$ ) to the physical space ( $x, y$ ). We can diagonalize the matrix  $\varepsilon_{(xy)}$  in Eq. (7) to get the principal axes and principal values.

We can also choose a more convenient method to calculate the material parameters for the interior of the branch cut: the effective medium theory (see, e.g., Ref. [29]). In effective medium theory, we can use alternating sub-wavelength layers of two isotropic media to represent an anisotropic medium via

$$\begin{aligned} \varepsilon_{\parallel} &= f \varepsilon_1 + (1 - f) \varepsilon_2 \\ \frac{1}{\varepsilon_{\perp}} &= \frac{f}{\varepsilon_1} + \frac{1-f}{\varepsilon_2} \end{aligned}, \quad (8)$$

where  $f$  is the filling factor,  $\varepsilon_1$  and  $\varepsilon_2$  are the two isotropic media, and  $\varepsilon_{\parallel}$  and  $\varepsilon_{\perp}$  are the two orthogonal components of the anisotropic medium. We choose  $\varepsilon_1 = \Delta/2$  and  $\varepsilon_2 = 2/\Delta$  and transform these locally isotropic media by the OCM. Then, we get the principal values of the transformed ONMs,

$$\begin{aligned} \varepsilon_{\parallel} &= \frac{1}{\Delta} \left| 1 - \frac{a^2}{z^2} \right| + \frac{\Delta}{4} \left| 1 - \frac{a^2}{z^2} \right| \approx \frac{1}{\Delta} \left| 1 - \frac{a^2}{z^2} \right| \\ \varepsilon_{\perp} &= \left| 1 - \frac{a^2}{z^2} \right| \frac{4\Delta}{\Delta^2 + 4} \approx \Delta \left| 1 - \frac{a^2}{z^2} \right| \end{aligned}. \quad (9)$$

Therefore,

$$\varepsilon_p = \left| 1 - \frac{a^2}{z^2} \right| \text{diag} \left( \frac{1}{\Delta}, \Delta, \Delta \right), \quad (10)$$

where  $\varepsilon_p$  ( $\varepsilon_p = \varepsilon_p$ ) represents the permittivity (permeability) tensor in the diagonalized form under the principal axis system. When  $\Delta$  approaches zero, Eq. (10) can be written as

$$\varepsilon_p = \mu_p = \text{diag}(\infty, 0, 0). \quad (11)$$

The shapes of the principal axes are the blue and white curves in Fig. 1(b), corresponding to the concentric rings in Fig. 1(a), under conformal mapping, as described in Eq. (1). Notably, the materials outside of the circular branch cut are isotropic, although inhomogeneous, while the materials inside of the circular branch cut are homogeneous, although anisotropic. In other words, unlike the well-known cloak based on transformation optics [4], our cloak does not need any complex material that is both anisotropic and inhomogeneous.



### III. SIMULATION

#### A. With ideal materials (under the assumption of weak dispersion)

First, we use numerical simulations to check whether our cloaks are omnidirectional and have a continuous working-frequency range under the assumption of weak dispersion (strong material dispersion is discussed in the following paragraph). We set  $\Delta = 1000$ ,  $a = 1$  m,  $R_1 = 0.1$  m, and  $R_2 = 4.1$  m in the following simulations. We also truncate the cloak to a circle with a radius of 8 m surrounded by a perfect matched layer (PML) with a thickness of 2 m. Plane waves with TE polarization are set as the source. To check the omnidirectional property, plane waves ( $\lambda = 1.5a$ ) with different incident angles of  $0^\circ$ ,  $45^\circ$ , and  $90^\circ$  impinge on two PMC objects (colored white) with the cloaks [Figs. 2(a)–2(c)] and without the cloaks [Figs. 2(d)–2(f)]. Actually, we can enclose any arbitrary objects (of arbitrary materials) that we want to conceal with the PMC boundary [of the gray region shape in Fig. 1(b)] to replace the PMC objects. From the results of the near-field patterns ( $E_z$ ), we find that nearly no scattering occurs using our cloak with these three incident angles, due to the phase-preserving mechanism of the ONMs, while obvious scatterings appear if we remove the cloaks. We also find good cloaking performance for other incident angles (not shown here). The two regions colored white in Fig. 2 are regions in which objects can be concealed. To verify whether the cloaks work under a continuous-frequency range, we choose three wavelengths ( $5a$ ,  $1.875a$ , and  $a$ ) randomly for the incident plane wave (with an incident angle of  $45^\circ$ ). The near-field patterns of cloaks are shown in Figs. 3(a)–3(c), and the magnified plots are shown in Figs. 3(d)–3(f).

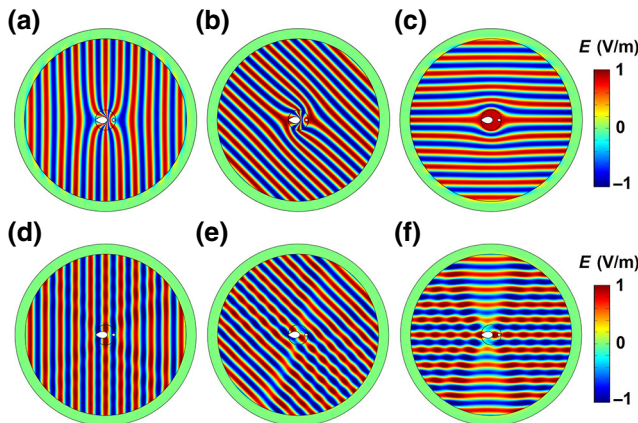


FIG. 2. Distributions of the  $z$  component of the electric field (TE) for the PMC objects (a)–(c) with the cloak and (d)–(f) without the cloak. Three incident angles are (a),(d):  $0^\circ$ , (b),(e):  $45^\circ$ , and (c),(f):  $90^\circ$ . The two regions colored white are the cloaking regions with PMC boundaries.

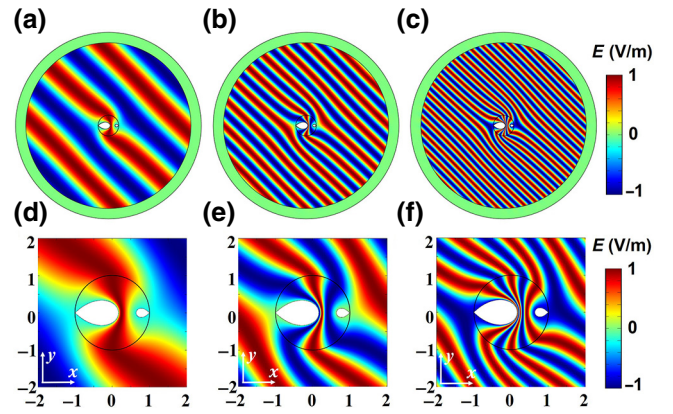


FIG. 3. Distributions of the  $z$  component of the electric field (TE) for the cloak under three random relative wavelengths of (a)  $5a$ , (b)  $1.875a$ , and (c)  $a$ . (d)–(f) are the magnified plots of those in (a)–(c). The two regions colored white are the cloaking regions with PMC boundaries.

We now provide a quantitative analysis for the cloaking performance by calculating the total scattering cross sections,  $\sigma$ , from the far-field results of the simulations. Since the geometry of the entire system has no rotational symmetry,  $\sigma$  is angle dependent. Four groups of plots are shown in Fig. 4 to give comparisons of the total scattering cross sections of the pure PMC, the PMC with our cloak, and the PMC with a conventional OCM cloak. The conventional OCM cloak used here for comparison has two mirrored Maxwell fish-eye lenses in the lower Riemann sheet, which has the following refractive index distribution inside the branch cut:

$$n(z) = \begin{cases} 1 - \frac{a^2}{z^2} \left| \frac{2}{1+|w-2a|^2/(2a)^2} |z| < a \& |w-2a| < 2a \right. \\ \left. \left| 1 - \frac{a^2}{z^2} \right| \frac{2}{1+|w+2a|^2/(2a)^2} |z| < a \& |w+2a| < 2a \right. \end{cases} \quad (12)$$

We use four plots that represent four different incident angles: (a)  $0^\circ$ , (b)  $30^\circ$ , (c)  $60^\circ$ , and (d)  $90^\circ$ . We set the  $y$  axis to the dB form of the total scattering cross sections per unit length for clarity, i.e.,  $\log_{10}(\sigma/1[\text{m}])$  dB, and the  $x$  axis represents the frequency, ranging from 0.02 to 0.3 GHz. It can be seen that the geometrical dispersion is removed and the total scattering cross sections are reduced by at least a factor of 100 (20 dB) for arbitrary angles and arbitrary frequencies, when covered by our cloaks (black curve), which are not achievable with the previous OCM cloaks (blue curve). No discrete frequencies are found in our simulations, and good cloaking effects are obtained for all frequencies. Under the same condition of weak material dispersion, our cloaks have a broad frequency band, while other conformal cloaks still have a discrete working frequency due to the geometrical dispersion.

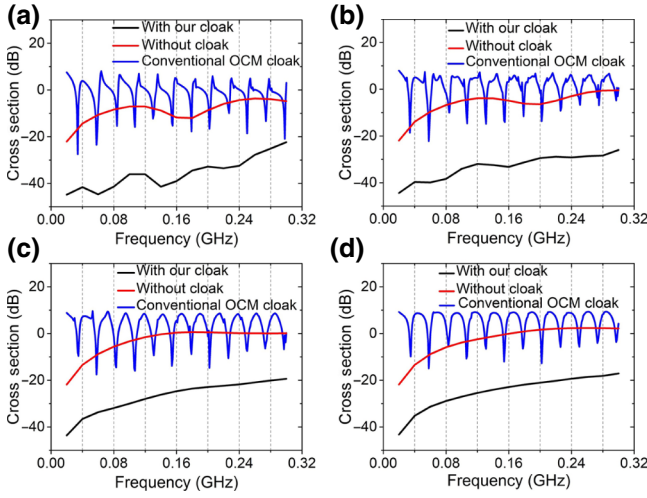


FIG. 4. Total scattering cross sections,  $\sigma$ , for the pure PMC (red), the PMC with our cloak (black), and the PMC with a conventional OCM cloak (blue) over a continuous range of frequencies (from 0.02 to 0.3 GHz) for different incident angles: (a)  $0^\circ$ , (b)  $30^\circ$ , (c)  $60^\circ$ , and (d)  $90^\circ$ .

### B. Realization of the cloak with metamaterials (under the assumption of strong dispersion)

Before studying the properties of strong dispersion of the ONM, we first show some potential ways to realize the proposed cloak. The realization of our cloak can be divided into two regions: outside the branch cut and inside the branch cut. The regions of our cloak outside the circular branch cut are isotropic materials, with an index from 0 to 2 [see Eq. (2); approaching vacuum in the far region], which we have studied in theory [18] and realized experimentally [14]. The regions inside the branch cut are ONMs with varied principal axes, which are experimentally realized in the microwave-frequency band [15,30]. One method to realize ONMs was proposed by Zhou's group [15], who used a well-designed photonic system composed of a porous metallic plate with a periodic array of subwavelength apertures to mimic an ONM. Another method, proposed by Chen's group [30], is to use the Fabry-Pérot resonances of a metallic slit array to mimic an ONM in a set of resonant frequencies. We can also use zero-index materials (ZIM) [31] and metal walls to mimic the ONM, i.e., the ZIM guarantees zero-phase advance and the metal walls prevent cross talk of each microchannel. For example, we can place perfect electrical conductors (PECs) along the principal axes of the ONMs and fill in the gaps with a ZIM, as shown in Fig. 5(a). In the magnified plot of Fig. 5(a), we can see that every two adjacent PEC boundaries and the ZIM between them form a microchannel, and no interference occurs between each of the microchannels, which ensures that the phases are the same between the incident and exit interfaces.

Now we show our cloak has a broader bandwidth compared with that of a conventional OCM cloak with the

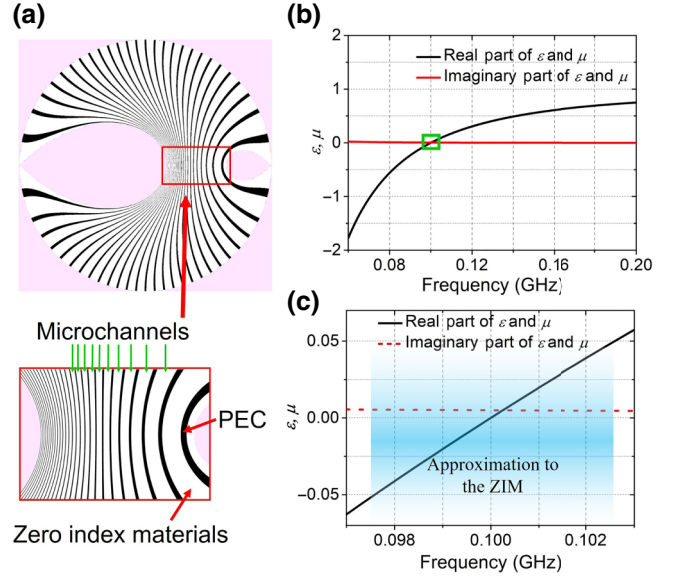


FIG. 5. One possible approach to realize our cloaks: using 27 microchannels composed of PECs and ZIMs. (a) Black curves and white gaps represent PEC boundaries and ZIMs, respectively. (b) Dispersion of the ZIM (Lorentz model). (c) Frequency band we use as ZIM (0.0975–0.1025 GHz).

same strong material dispersion (using the Lorentz model). In this case, the parameters of the ZIM are replaced by the Lorentz model, which is given by

$$\varepsilon(\omega) = \mu(\omega) = 1 + \omega_p^2 \frac{\omega_0^2 - \omega^2 + i\gamma\omega}{(\omega_0^2 - \omega^2)^2 + \gamma^2\omega^2}, \quad (13)$$

where  $\omega_p/2\pi = 0.1$  GHz,  $\omega_0/2\pi = 0.0005$  GHz, and the damping coefficients (representing the material loss)  $\gamma/2\pi = 0.0005$  GHz. The dispersion curves are shown in Figs. 5(b) and 5(c).

The reference we use here is a conventional OCM cloak, with two mirrored Maxwell fish-eye lenses in the lower Riemann sheet [17,18], which has both geometrical dispersion and material dispersion (the Lorentz model is also used to mimic the large permittivity range, 0–160, inside the branch cut). To match the boundary conditions, we replace the TE wave with a TM wave and change the materials outside of the circular branch cut with the following replacement:  $(\varepsilon = n^2, \varepsilon = 1) \rightarrow (\varepsilon = 1, \varepsilon = n^2)$ . Figure 6(a) shows the total scattering cross sections for the PEC with our cloak (with 27 microchannels), the pure PEC, and the PEC with a conventional OCM cloak. The corresponding field patterns at some frequencies are shown in Figs. 6(b)–6(g). Notably, the narrow bandwidth of the conventional OCM cloak (red curve) originates from both the geometrical dispersion and the material dispersion. The inconsistent change of refractive index with frequency shifts usually makes the refractive index

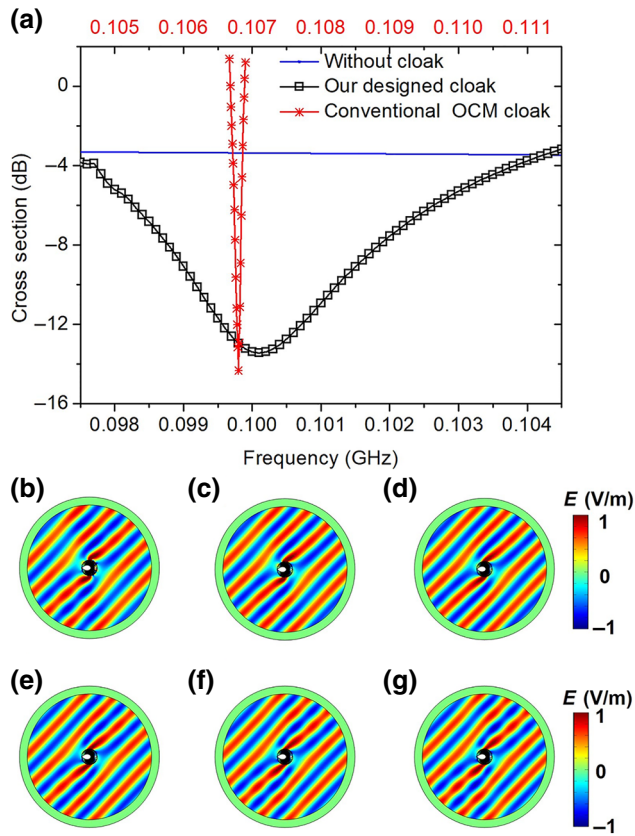


FIG. 6. (a) Total scattering cross sections for the pure PEC (blue), the PEC with a conventional OCM cloak (red), and the PEC with our cloak (black) in a frequency band from 97.5 to 104.5 MHz. (b)–(g) Electric field distribution ( $E_x$ ) in a frequency band: (b) 0.098 GHz, (c) 0.099 GHz, (d) 0.100 GHz, (e) 0.101 GHz, (f) 0.102 GHz, and (g) 0.103 GHz.

distribution completely disordered (away from the theoretical cloak design), even with a tiny frequency shift, i.e., its cloak performance is more sensitive to a frequency shift.

In Fig. 6(a), all parameters of the conventional OCM cloak are adjusted to an accurate value [Eq. (12)] at a fixed frequency, and therefore, we can see a cloaking effect (the red dip). However, in the process of fabrication, the machining error makes each unit cell deviate slightly from its original shape, i.e., we cannot adjust the unit cell to an accurate value as we do in the simulation at any frequency. Therefore, we cannot find a single frequency where we can see the cloaking effect for a conventional OCM cloak. On the contrary, our cloak only uses one unit cell, and we can still find a cloaking effect in a neighboring frequency range, even if the unit cell deviates from its designed shape. Therefore, our cloak is more robust to fabrication errors.

#### IV. DISCUSSION

##### A. Reduction of the material dispersion

Previous OCM cloaks have both geometrical dispersion and material dispersion. Although the geometrical

dispersion is fixed in our design, the material dispersion of a passive ZIM still limits the bandwidth of our cloak. The bandwidth can be improved, such as using broadband zero-index materials [32–34]. Although passive cloaks have some bandwidth limitations [35], active zero-index materials can be an effective way to fix the material dispersion problem and further broaden the bandwidth of our cloak [36]. Another way to reduce the material dispersion on our cloak is to realize the ONM without using a ZIM. Some studies realize the ONM without using a ZIM [37], and here we use a similar method to make some reduction to our cloak by replacing the ZIM with normal dielectrics for a refractive index ranging from one to two, which can be easily realized using materials with weak dispersion.

##### B. Practical realization of a simplified cloak

From the above discussion, we can see the most difficult part, preventing the practical realization of the cloak, lies in the ZIMs of each microchannel, which is also the principal part limiting the bandwidth. We now replace the ZIMs using normal dielectrics to simplify the cloak. By proper choice of the refractive index of each microchannel, i.e., ensuring the optical path in each microchannel to be integer multiples of the wavelength, we can also obtain a satisfactory cloaking effect. Here, the designed working frequency is 0.305 GHz and the designed refractive index value for each of the 27 microchannels is shown in Fig. 7(a), which ranges from one to two. Figure 7(b) shows the total scattering cross sections per unit length for the bare PEC without a cloak (red), the PEC with an ideal ONM cloak (blue), and the PEC with a simplified cloak (black). We can see that our simplified cloak still has a good cloak performance within a bandwidth of about 10%. However, the materials inside the branch cut are greatly simplified to isotropic dielectrics (homogenous in each microchannel) with a refractive index ranging between one and two, which can be easily realized using materials with weak dispersion. Our simplified cloak is composed of three

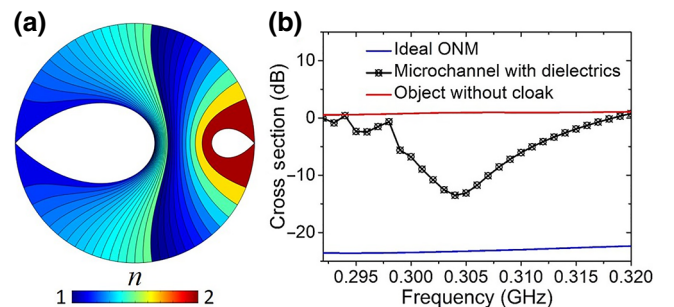


FIG. 7. (a) Refractive index distribution inside the branch cut of the simplified cloak (homogenous in each microchannel). (b) The total scattering cross sections of the bare PEC without a cloak (red), the PEC with an ideal ONM cloak (blue), and the PEC with a simplified cloak (black).



parts: metal boundaries inside the branch cut, magnetic materials outside the branch cut, and dielectrics inside each metal boundaries, which can be practical realized by metal walls and ordinary magnetic and dielectric slabs with holes, respectively. We can realize our cloak from ordinary materials without using metamaterials with complex structures. Therefore, our cloaking method will play a role in promoting more practical invisibility technology.

## V. CONCLUSION

By introducing an optically null medium during optical conformal mappings, we can design an omnidirectional two-dimensional cloak using ZIMs to eliminate the geometrical dispersion. It is also possible to use normal dielectrics (resonant microchannels) instead of the ZIMs to achieve a more practical cloak with a relaxed requirement (with geometrical dispersion). The latter has more practical applications, e.g., two-dimensional on-chip optical systems; our cloak can isolate some special components from the surrounding light waves and, at the same time, it will not break the original optical signal transmission path. The fabrication of curved metal walls will become easier with the development of micro- and nanoprocessing technology, which contributes to the realization of our omnidirectional cloak.

In conclusion, we solve two major issues of OCM cloaks: (1) geometrical dispersion, which determines the fixed discrete working frequency; and (2) the large refractive index range in the interior of the branch cut, which originates from the conformal transformation ( $w = z + a^2/z$ ; mapping an infinite plane to the interior of a circle). We change these materials to homogenous ONMs or normal dielectrics. Our cloaks have the following advantages: first, no phase-delay problem: the geometrical dispersion is removed and the bandwidth is improved; second, more robust to fabrication errors; third, our cloak does not require any complex material that is both anisotropic and inhomogeneous; and fourth, the cloaks are omnidirectional. Our method can also extend to other OCM devices and to two-dimensional on-chip photonic systems, e.g., cross-talk-free and zero-phase advance waveguides.

## ACKNOWLEDGMENTS

This work is partially supported by the National Natural Science Foundation of China (Grants No. 61905208, No. 61971300, No. 11604292, No. 11674239, No. 91833303, No. 11621101, No. 91233208, No. 6099032211604292, No. 11621101, No. 91233208, No. 11621101, and No. 60990322), the Scientific and Technological Innovation Programs (STIP) of Higher Education Institutions in Shanxi (Grants No. 2019L0146 and No. 2019L0159), the Postdoctoral Science Foundation of China (Grants No. 2018M632455 and No. 2017T100430), the National Key Research and Development Program of China (Grant

No. 2017YFA0205700), the Program of Zhejiang Leading Team of Science and Technology Innovation, and AOARD.

- 
- [1] H. Y. Chen, C. T. Chan, and P. Sheng, Transformation optics and metamaterials, *Nat. Mater.* **9**, 387 (2010).
  - [2] F. Sun, B. Zheng, H. Chen, W. Jiang, S. Guo, Y. Liu, Y. Ma, and S. He, Transformation optics: From classic theory and applications to its new branches, *Laser Photonics Rev.* **22**, 1700034 (2017).
  - [3] A. Greenleaf, Y. Kurylev, M. Lassas, and G. Uhlmann, Cloaking devices, electromagnetic wormholes, and transformation optics, *SIAM Rev.* **51**, 3 (2009).
  - [4] J. B. Pendry, D. Schurig, and D. R. Smith, Controlling electromagnetic fields, *Science* **312**, 1780 (2006).
  - [5] U. Leonhardt, Optical conformal mapping, *Science* **312**, 1777 (2006).
  - [6] U. Leonhardt and T. G. Philbin, Chapter 2 transformation optics and the geometry of light, *Prog. Opt.* **53**, 69 (2009).
  - [7] J. Valentine, J. Li, T. Zentgraf, G. Bartal, and X. Zhang, An optical cloak made of dielectrics, *Nat. Mater.* **8**, 568 (2009).
  - [8] T. Ergin, N. Stenger, P. Brenner, J. B. Pendry, and M. Wegener, Three-dimensional invisibility cloak at optical wavelengths, *Science* **328**, 337 (2010).
  - [9] L. H. Gabrielli, J. Cardenas, C. B. Poitras, and M. Lipson, Silicon nanostructure cloak operating at optical frequencies, *Nat. Photonics* **3**, 461 (2009).
  - [10] R. Liu, C. Ji, J. J. Mock, J. Y. Chin, T. J. Cui, and D. R. Smith, Broadband ground-plane cloak, *Science* **323**, 366 (2009).
  - [11] B. Zhang, Y. Luo, X. Liu, and G. Barbastathis, Macroscopic Invisibility Cloak for Visible Light, *Phys. Rev. Lett.* **106**, 033901 (2011).
  - [12] D. Schurig, J. J. Mock, B. J. Justice, S. A. Cummer, J. B. Pendry, A. F. Starr, and D. R. Smith, Metamaterial electromagnetic cloak at microwave frequencies, *Science* **314**, 977 (2006).
  - [13] U. Leonhardt, Notes on conformal invisibility devices, *New J. Phys.* **8**, 118 (2006).
  - [14] Y. G. Ma, Y. C. Liu, L. Lan, T. T. Wu, W. Jiang, C. K. Ong, and S. L. He, First experimental demonstration of an isotropic electromagnetic cloak with strict conformal mapping, *Sci. Rep.* **3**, 2182 (2013).
  - [15] Q. He, S. Y. Xiao, X. Li, and L. Zhou, Optic-null medium: Realization and applications, *Opt. Express* **21**, 28948 (2013).
  - [16] S. Fei and S. He, Optical surface transformation: Changing the optical surface by homogeneous optic-null medium at will, *Sci. Rep.* **5**, 16032 (2015).
  - [17] Q. N. Wu, Y. D. Xu, H. Li, and H. Y. Chen, Cloaking and imaging at the same time, *EPL* **101**, 34004 (2013).
  - [18] Y. Liu, M. Mukhtar, Y. Ma, and C. K. Ong, Transmutation of planar media singularities in a conformal cloak, *J. Opt. Soc. Am.* **30**, 2280 (2013).
  - [19] F. Sun and S. He, Can Maxwell's fish eye lens really give perfect imaging?, *Prog. Electromagn. Res.* **108**, 307 (2010).
  - [20] U. Leonhardt, Perfect imaging without negative refraction, *New J. Phys.* **11**, 093040 (2009).

- [21] T. Xu, Y. C. Liu, Y. Zhang, C. K. Ong, and Y. G. Ma, Perfect invisibility cloaking by isotropic media, *Phys. Rev. A* **86**, 3076 (2012).
- [22] Q. N. Wu, X. Y. Feng, R. R. Chen, C. D. Gu, S. C. Li, H. Li, Y. D. Xu, Y. Lai, B. Hou, H. Y. Chen, and Y. H. Li, An inside-out Eaton lens made of H-fractal metamaterials, *Appl. Phys. Lett.* **101**, 031903 (2012).
- [23] M. Yin, X. Yong Tian, L. Ling Wu, and D. Chen Li, All-dielectric three-dimensional broadband Eaton lens with large refractive index range, *Appl. Phys. Lett.* **104**, 188 (2014).
- [24] Y. Liu, F. Sun, and S. He, Controlling lightwave in Riemann space by merging geometrical optics with transformation optics, *Sci. Rep.* **8**, 514 (2018).
- [25] H. Chen, U. Leonhardt, and T. Tyc, Conformal cloak for waves, *Phys. Rev. A* **83**, 10017 (2011).
- [26] H. Li, Y. Xu, and H. Chen, Conformal cloaks at eigenfrequencies, *J. Phys.* **46**, 135109 (2013).
- [27] F. Sun and S. L. He, Extending the scanning angle of a phased array antenna by using a null-space medium, *Sci. Rep.* **4**, 6832 (2014).
- [28] F. Sun, Y. Zhang, J. Evans, and S. He, A camouflage device without metamaterials, *Prog. Electromagn. Res.* **165**, 107 (2019).
- [29] S. M. Rytov, Electromagnetic properties of a finely stratified medium, *Sov. Phys. JETP* **29** (1956).
- [30] M. M. Sadeghi, S. Li, X. Lin, H. Bo, and H. Chen, Transformation optics with fabry-pérot resonances, *Sci. Rep.* **5**, 8680 (2015).
- [31] I. Liberal and N. Engheta, Near-zero refractive index photonics, *Nat. Photonics* **11**, 149 (2017).
- [32] P. Moitra, Y. Yang, Z. Anderson, I. I. Kravchenko, D. P. Briggs, and J. Valentine, Realization of an all-dielectric zero-index optical metamaterial, *Nat. Photonics* **7**, 791 (2013).
- [33] L. Sun, J. Gao, and X. Yang, Broadband epsilon-near-zero metamaterials with steplike metal-dielectric multilayer structures, *Phys. Rev. B* **87**, 1 (2013).
- [34] L. Sun, X. Yang, and J. Gao, Loss-compensated broadband epsilon-near-zero metamaterials with gain media, *Appl. Phys. Lett.* **103**, 213902 (2013).
- [35] H. Hashemi, C. W. Qiu, A. P. McCauley, J. D. Joannopoulos, and S. G. Johnson, Diameter-bandwidth product limitation of isolated-object cloaking, *Phys. Rev. A* **86**, 013804 (2012).
- [36] K. W. Yu and L. Sun, Strategy for designing broadband epsilon-near-zero metamaterials, *J. Opt. Soc. Am.* **29**, 984 (2012).
- [37] F. Sun, S. Guo, Y. Liu, and S. He, A magnifying glass for virtual imaging of subwavelength resolution by transformation optics, *Adv. Mater.* **30**, 1801641 (2018).